(Received 9 February 2026, Accepted 8 May 2026, Scheduled 27 June 2026)

Accelerating Field Decay along Nonlocal Metasurfaces by Suppressing the Norton Wave

Alexander Zhuravlev*, Dmitry Tatarnikov, Yury Kurenkov, and Stanislav Glybovski

School of Physics and Engineering, ITMO University, St. Petersburg, Russia

ABSTRACT: Investigations into the nature of electromagnetic fields produced by dipole sources over homogeneous flat ground or impedance surfaces date back many years. In general, at a long distance r from the source, the near-surface field is mostly contributed by the geometrical optics term (describing the radiation pattern), a guided wave, and a higher-order reactive contribution referred to as the Norton wave. In the special case of a perfect magnetic conductor interface, the first two terms vanish; thus, the residual Norton wave determines the steepest achievable field decay profile of $r^{-3/2}$ (for a two-dimensional horizontal magnetic dipole). In this paper, we reveal that in the presence of a non-local metasurface described by the second-order impedance boundary condition, the field decay can be further accelerated by suppressing the Norton wave (approaching the profiles $r^{-5/2}$ and $r^{-7/2}$ for the electric and magnetic fields, respectively). In a proposed practical realization of a nonlocal metasurface, the effect is numerically verified and shown to reduce the edge diffraction effects by 10 dB for a shield diameter of only one wavelength, paving the way for compact antenna systems.

1. INTRODUCTION

The electromagnetic field solution for a dipole source above a lossy dielectric boundary (Sommerfeld's problem) is a classical model of an antenna operating over the Earth at radio frequencies [1–3] or a nano-antenna over a plasmonic metal-air interface in the optical regime [4, 5]. The asymptotics of the exact solution (in the form of Sommerfeld-like integrals) commonly used in the literature to analyze the near-surface field behavior at a long distance r from the source, in general, contains the following contributions: (i) the geometrical optics (GO) term (related to the radiation pattern) with a decay profile of r^{-1} (in a 3D problem) or $r^{-1/2}$ (in a 2D problem); (ii) higher-order terms in a power series of r^{-1}, including the so-called Norton wave decaying as r^{-2} (in a 3D problem) [3] or $r^{-3/2}$ (in a 2D problem) [5], which describe reactive fields; and (iii) the guided wave typically having the form of a trapped (surface) wave. The interplay between the above terms substantially defines the near-surface field profile far from the source.

Metasurfaces (MSs, two-dimensional periodic structures with subwavelength periodicity) serve as platforms for synthesizing desired scattered-field distributions under a given excitation [6]. The local response of an impenetrable (impedance) MS can be described at the macroscopic level with a frequency-dependent surface impedance Z_s, which connects the averaged tangential electric E_t and magnetic H_t fields at the same point on the MS through the Leontovich boundary condition: $E_t = Z_s H_t$. The most popular realizations of such local MSs are corrugated [7] and mushroom-type [8] surfaces, for which $|Z_s| \gg \eta$ near the resonance, where η is the characteristic impedance of free space. Such so-called high-impedance surfaces (HISs) serve as artificial magnetic conductor (AMC) reflectors for propagating plane waves and simultaneously suppress any propagating surface waves (the electromagnetic band gap (EBG) property) [8]. For a dipole source above a local MS with an arbitrary Z_s, an asymptotic representation of the near-surface field with the same types of waves as for the lossy dielectric is valid [9]. The limiting case $Z_s = 0$ corresponds to a perfect electric conductor (PEC) ground plane, for which the GO term dominates in the asymptotic behavior of a field excited by an in-plane (located at a small height h compared to wavelength λ) horizontal magnetic dipole (HMD), whereas no guided wave is supported [see Fig. 1(a)]. In another limit, when $Z_s \to \infty$, mimicking the perfect magnetic conductor (PMC) boundary, the GO term is zero because of the destructive interference between the HMD and its mirror image, whereas still no propagating guided wave is supported. Consequently, the main contribution to the near-surface field is the Norton wave [Fig. 1(b)]. Owing to a faster field decay than that of the PEC ground plane ($r^{-3/2}$ vs. $r^{-1/2}$ for a 2D problem [10]), HISs near the resonance serve as compact antenna shields with improved suppression in the shadow domain [11–13] and decoupling structures [14].

For a more general nonlocal MS response, E_t and H_t at different points are related to each other [15]. Nonlocality manifests itself in the spatial dispersion (SD) of Z_s, that is, its variation with the incident wave vector [16]. Adjusting SD law has been shown to control the angular properties of MS absorbers [17], antenna reflectors [18], and the transmittance of the anti-reflection coating [19]. Although the problem of dipole excitation of spatially dispersive wire grids [20] and plasmonic metal boundaries [5] has been solved analytically, to our knowledge, the possibility of systematically controlling and accelerating the field decay along the MS has not been studied.

* Corresponding author: Alexander Zhuravlev (a.zhuravlev@metalab.ifmo.ru).

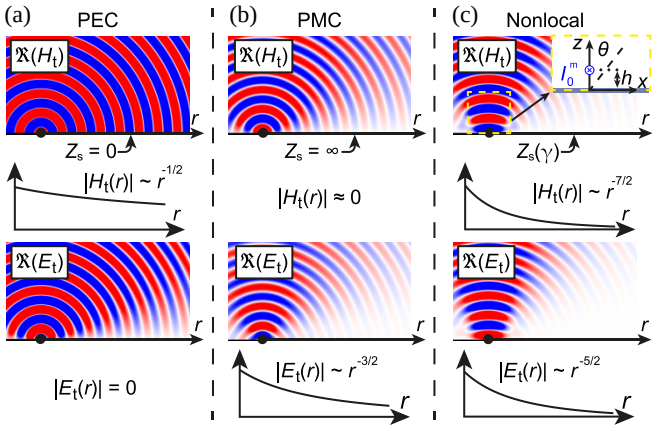

FIGURE 1. Fields excited by an HMD placed at height $h \ll \lambda$ above a (a) PEC, (b) PMC, and (c) nonlocal impedance boundary with an impedance pole at a grazing angle $\gamma = \sin\theta = 1$. The geometry of the 2D problem considered is depicted in the inset of (c).

Here, we further study 2-D nonlocal MSs by considering the field distribution along the MS, which is illuminated by a magnetic line current (MLC) and modeled by the second-order boundary condition (SOBC), which approximates the surface impedance of the MS, $Z_s(\gamma)$, where $\gamma = \sin\theta$, by a second-order rational function of the incident angle. We analytically show that a specific set of SOBC coefficients that induces a second-order pole in the surface impedance at grazing angles nullifies the Norton wave. In the absence of the former, the leaky wave (LW) contribution remains dominant near the MLC; however, the next algebraic terms decay as $r^{-5/2}$ for the electric field and as $r^{-7/2}$ for the magnetic field [see Fig. 1(c)]. This rapid field decay enables key practical applications, such as reducing edge effects in shielded antennas and improving isolation between closely spaced sources. As an example of the former, we numerically demonstrate that the nonlocal approach improves the shielding performance of one-wavelength HISs by 10 dB compared with the local design.

2. FIELDS ALONG LOCAL AND NONLOCAL IMPEDANCE BOUNDARIES

To investigate the near-surface field decay in the presence of nonlocality, we consider a 2D problem with an infinite magnetic line current of complex amplitude I_0^m (a 2D dipole oriented along the y axis) at height $h \ll \lambda$ above a uniform and isotropic MS. The latter is located in the XY plane and is modeled by a spatially dispersive surface impedance $Z_s(\gamma)$, as shown in the inset of Fig. 1(c). The source generates a TM$_y$-polarized field with only H_y, E_x, and E_z components that are nonzero. The tangential components of the total field $E_t = E_x$, $H_t = H_y$ (the sums of the incident and reflected fields), observed at angle $0 \le \theta \le 90°$ and distance r from the source, have the following rigorous spectral representations [21, Section 5]:

$$\begin{Bmatrix} E_x(\theta) \\ H_y(\theta) \end{Bmatrix} = \frac{C}{\sqrt{2\pi}} \int_P f_{\{E_x,H_y\}}(\tau) e^{-j\Omega\cos(\tau-\theta)} d\tau, \quad (1)$$

where τ is related to the normalized tangential wave vector component $\gamma = k_x/k$ of a spatial spectrum harmonic as $\sin\tau = \gamma$ (harmonics with $0 \le \gamma \le 1$ and $0° \le \tau = \theta \le 90°$ are propagating plane waves, whereas harmonics with $\gamma > 1$ are evanescent plane waves); $C = I_0^m k/\sqrt{2\pi}\eta$; k is the wavenumber of free space; $\Omega = kr$; $r = \sqrt{x^2 + (z-h)^2}$; P is the contour of integration (depicted in [the Supplementary Information (SI) Fig. S.1]); and the integrated functions are determined by the SD law $Z_s(\gamma)$ as follows:

$$f_{H_y} = \frac{-\cos\tau}{Z_s(\sin\tau)/\eta + \cos\tau}; \quad f_{E_x} = -Z_s(\sin\tau) f_{H_y}. \quad (2)$$

A far-field approximation ($\Omega \gg 2\pi$) of (1) for a specific observation angle $\tau = \theta \le 90°$ can be derived using the steepest descent method[1] [21, Ch. 4]:

$$\begin{Bmatrix} E_x(\theta) \\ H_y(\theta) \end{Bmatrix} \approx Ce^{-j\left(\Omega-\frac{\pi}{4}\right)} \Bigg(\underbrace{\begin{Bmatrix} f_{E_x}(\theta) \\ f_{H_y}(\theta) \end{Bmatrix} \frac{1}{\Omega^{\frac{1}{2}}}}_{\text{GO term}} + \sum_{n=1}^{\infty} \underbrace{j^n f^{(2n)}_{\{E_x,H_y\}}(\theta) \frac{(2n-1)!!}{(2n)!}}_{F_{n,\{E_x,H_y\}}} \frac{1}{\Omega^{\frac{2n+1}{2}}} \Bigg) - \underbrace{\sum_i \begin{Bmatrix} E^{\mathrm{GW}}_{x,i} \\ H^{\mathrm{GW}}_{y,i} \end{Bmatrix} e^{-j\Omega\cos(\tau_i-\theta)}}_{\text{Guided waves}}, \quad (3)$$

where $f^{(2n)}(\theta)$ denotes the derivative of $2n$-th order with respect to θ, and "GW" denotes guided waves.

In (3), the first term is the GO term, for which functions (2) for $0° \le \tau = \theta \le 90°$ determine the radiation pattern. The next term ($n = 1$) is the Norton wave, which, along with other higher-order terms ($n \ge 2$) exhibits an algebraic dependence on the distance Ω. The last sum in (3) of terms exponentially dependent on the distance, resulting from the poles of (2) with respect to τ, accounts for the contribution of guided waves with excitation amplitudes $E^{\mathrm{GW}}_{x,i}$, $H^{\mathrm{GW}}_{y,i}$. Depending on the roots τ_i of the characteristic equation, that is, the denominator of (2) equals zero, guided waves may be surface waves (SWs for $\sin\tau_i \in \mathbb{R}$) or leaky waves (LWs for $\sin\tau_i \in \mathbb{C}$).

Consider the fields near the MS plane. Both f_{E_x} and f_{H_y} vanish at $\theta \to 90°$ for all SD laws, except those that satisfy condition $Z_s(90°) = 0$, so that the GO term in (3) becomes zero. However, the contribution of other asymptotic terms strongly depends on the SD of Z_s. We now find the specific conditions under which the fields $E_x(90°)$, $H_y(90°)$ decay fastest with Ω. Clearly, no SWs should be supported by the MS, whereas the Norton wave and LWs should be minimized or canceled.

Following [18, 23–25], we assume the MS to be lossless and represent its purely imaginary impedance $Z_s(\gamma)$ as a rational

[1] It is worth noting that we evaluate nonuniform asymptotic, which is valid when the contributions of the special points (the saddle point and the poles of the integrand in our study) are well separated in the complex τ-plane [22].

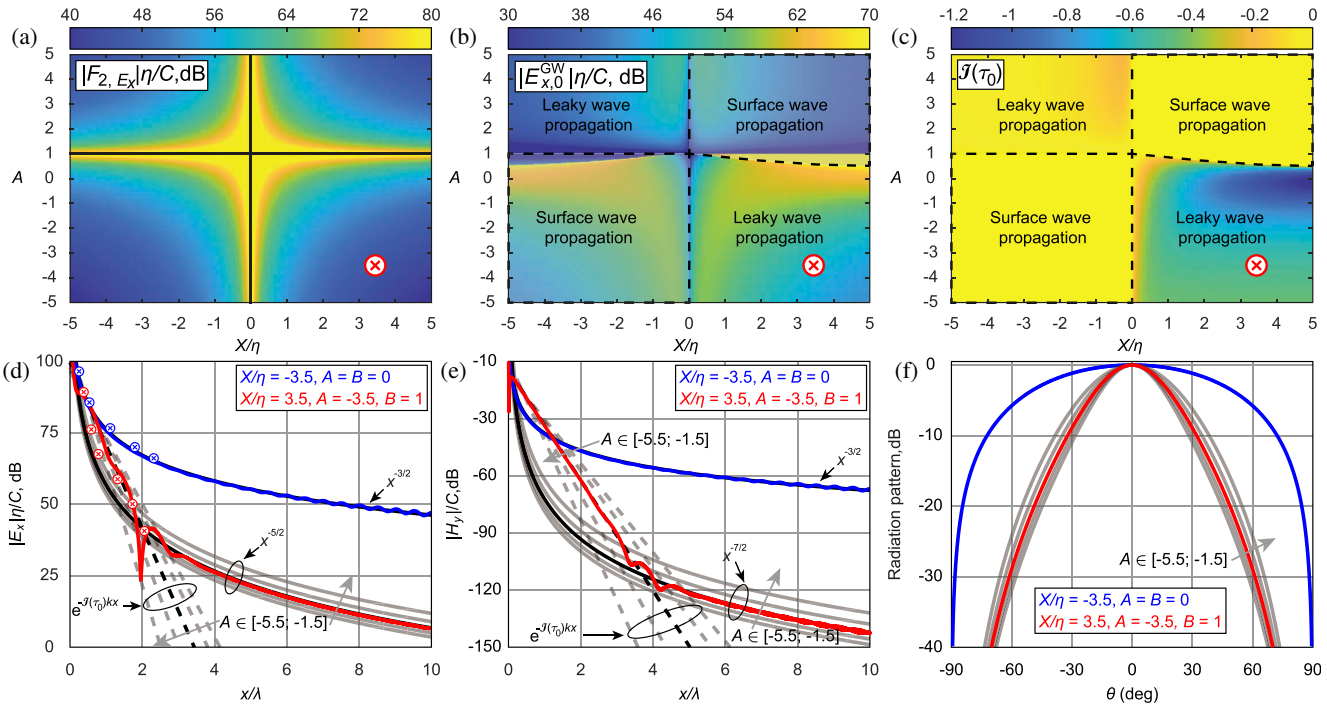

FIGURE 2. Analytical study of fields excited by a 2D HMD on a nonlocal MS with a surface impedance of (4) with $B = 1$ (Norton wave suppressed) depending on A and X/η: (a) normalized excitation coefficient level $|F_{2,E_x}|\eta/C$ of the term decaying as $E_x \sim \Omega^{-5/2}$; (b) normalized excitation coefficient level $|E^{\mathrm{GW}}_{x,0}|\eta/C$ of a SW/LW; (c) exponential decay factor $\Im(\tau_0)$ of the LW (SW propagation regions are uniformly yellow); normalized levels of the tangential electric (d) and magnetic (e) field (solid lines) calculated with (1) vs. distance from the source x/λ compared with their dominating asymptotic expansion terms from (3); (f) radiation pattern shape. The case with the set of parameters $B = 1$, $A = -3.5$, $X/\eta = 3.5$, chosen for the practical implementation, is indicated with cross markers in (a)–(c) and with red lines in (d)–(f). The local high-impedance case is shown in (d)–(f) with blue curves. Markers in (d) show the results of full-wave numerical confirmation for the practical MS implementation.

function, for which a second-order Padé approximation with one zero and one pole is [18]:

$$Z_s(\gamma) = jX\frac{1-\sum_{n=1}^{\infty}A_n\gamma^{2n}}{1-\sum_{m=1}^{\infty}B_m\gamma^{2m}} \approx jX\frac{1-A\gamma^2}{1-B\gamma^2}, \quad (4)$$

where $A \neq 1$, $X \neq 0$ (to maintain the GO term at zero), and $B \neq A$ (to keep the nontrivial SD law). In the lossless case, all the above-mentioned coefficients are real numbers; in the presence of losses, they become complex-valued, and to keep surface impedance meaningful, one needs to choose the signs of the imaginary part to satisfy $\Re(Z_s(\gamma)) > 0$ for any γ. Moreover, the frequency dispersion of the coefficients should provide $Z_s(\gamma)$ that satisfies Foster's reactance theorem at any γ [23]. Note that when $A = B = 0$, the value of $Z_s(\gamma)$ becomes constant with γ (hereafter referred to as a *local* case). As seen in (3), the electric and magnetic field amplitudes of the Norton wave $F_{1,\{E_x,H_y\}}$ (the term with $n = 1$) are proportional to the second-order derivatives of f_{E_x} and f_{H_y}, respectively, at $\theta = 90°$. Considering (4), the derivatives can be expressed as follows:

$$f''_{H_y} = -\frac{2\eta^2}{X^2}\frac{(B-1)^2}{(A-1)^2}; \quad f''_{E_x} = \frac{2j\eta^2}{X}\frac{(B-1)}{(A-1)}. \quad (5)$$

Both expressions in (5) show that the Norton wave cancels with the choice $B = 1$ (a second-order pole of the impedance is set at the grazing angle $\theta = 90°$). In this case, the next nonzero contributions in (3) are $E_x \sim \Omega^{-5/2}$ and $H_y \sim \Omega^{-7/2}$, as well as of a single guided wave[2] (with a complex propagation factor of τ_0 satisfying the characteristic equation). As noted in [18], F_{0,H_y} determines the radiation pattern, which for $B = 1$ is proportional to $\cos^3\theta$, as follows from (2) and (4). For comparison, the radiation pattern for the PMC is proportional only to $\cos\theta$. This means that the Norton wave suppression is expected to be accompanied by the radiation pattern narrowing.

The analytically calculated[3] levels of F_{2,E_x} (for the contribution $E_x \sim \Omega^{-5/2}$), as well as the excitation coefficient $E^{\mathrm{GW}}_{x,0}$ and the decay factor $\Im(\tau_0)$ of the GW, are shown in Figs. 2(a)–(c) in the case $B = 1$ (Norton wave suppressed) for different A and X/η. As follows from Fig. 2(a), by simultaneously increasing both $|A|$ and $|X|$, one can decrease the contribution $E_x \sim \Omega^{-5/2}$ to the overall tangential electric field profile. On the other hand, for some combinations of A and X, a propagating surface wave may appear (see the yellow regions in Fig. 2(c) that must be avoided). For other combinations of A and X, the guided wave becomes an LW with $\Im(\tau_0)$ strongly dependent on both A and X. Although for $X < 0$ and $A > 0$, the LW has a relatively small amplitude, it has the slowest decay. Therefore,

[2]For quadratic surface impedance, dispersion relation [Eq. (S.5) in the SI] generally has three solutions: one corresponding to a SW and two complex-conjugate roots corresponding to LWs. During our study, we identified two distinct cases: propagation of an SW or an LW.

[3]The corresponding excitation coefficients F_{2,E_x}, F_{3,H_y}, $E^{\mathrm{GW}}_{x,0}$, and $H^{\mathrm{GW}}_{y,0}$ as well as propagation factor τ_0 can be analytically calculated using Eqs. (S.1)–(S.5) from the SI.

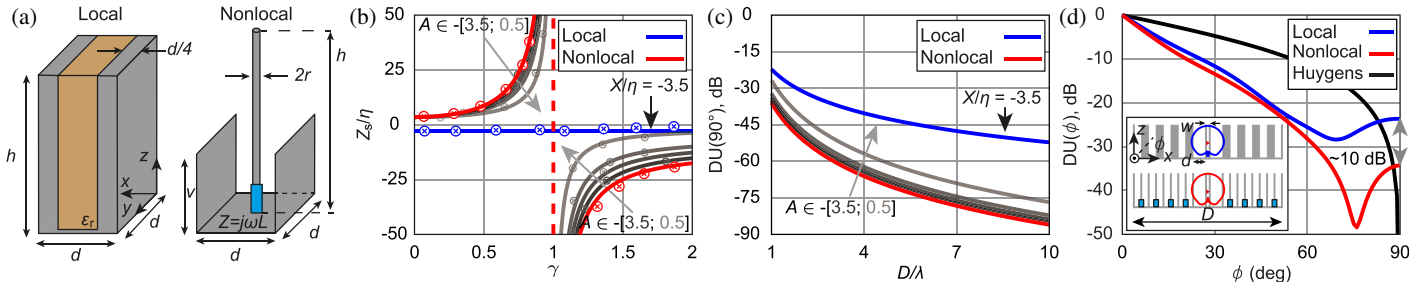

FIGURE 3. Comparison of practical implementations of the local and nonlocal MSs: (a) meta-atoms of the local corrugated HIS (left) and the proposed nonlocal MS (right), (b) numerically extracted (markers) and analytically calculated (solid lines) $Z_s(\gamma)$, (c) analytically estimated DU(90°) for $X/\eta = 3.5$, $B = 1$, and different practically implementable negative values of A (see [the SI Tab. S.1]), and (d) full-wave numerically calculated DU(ϕ) for $D = \lambda$.

to accelerate the overall decay along the MS, it is preferable to select a larger positive X together with a negative A.

The contributions of the asymptotic term with $E_x \sim \Omega^{-5/2}$ (solid gray curves) and LW (dashed gray curves) for different negative values of A are plotted versus distance x/λ along the MS in Fig. 2(d)[4]. For the particular case $A = -3.5$, the asymptotic profiles are shown with black curves, while the total tangential electric field profile calculated using (1) is shown with the solid red curve. It is clearly seen that at small distances ($x/\lambda < 1.5$) the field decay is mainly determined by the LW, while at large distances ($x/\lambda > 3$) it strictly follows the $E_x \sim \Omega^{-5/2}$ profile. In the middle range of distances, an interference of different wave contributions can be observed. A similar conclusion on the dominance of the term $H_y \sim \Omega^{-7/2}$ or LW, depending on the distance, can be drawn for the magnetic field profile shown in Fig. 2(e). For comparison, the profiles of electric and magnetic fields excited by the same source calculated using (1) are presented on the same plots for the local high-impedance MS with $X/\eta = -3.5$ along with asymptotic terms [Eqs. (S.6)–(S.7) from the SI]. Note that in this case, guided waves cannot be excited by the TM-polarized source due to capacitive impedance [26, Par. 6.4.5], hence the field profiles precisely follow the contribution of the Norton wave ($E_x \sim \Omega^{-3/2}$). This comparison shows that for $x/\lambda > 2$, despite some LW excitation, the field levels on the nonlocal MS with $B = 1$ remain drastically lower than those for the local MS, which can be explained by the Norton wave suppression. Furthermore, Fig. 2(f) confirms that the Norton wave suppression on nonlocal MSs is associated with a significantly narrower beam (especially for larger $|A|$) pointed in the normal direction.

3. SHIELDING PERFORMANCE OF FINITE LOCAL AND NONLOCAL METASURFACES

To confirm the analytical predictions of the field decay acceleration, we numerically compare the excitation of two practical periodic structures implementing local and nonlocal MSs with the same period $d = \lambda/10 = 3\,\text{mm}$ at a frequency of $f = 10\,\text{GHz}$ and the same thickness $h = 6.2\,\text{mm}$. The local MS is implemented as a corrugated surface [7, 12] with dielectric-filled ($\varepsilon_r = 1.6$) PEC grooves [see Fig. 3(a)]. The nonlocal MS is implemented as a modification of the HIS formed by vertical metal pins of height h [27–29], where the pins with a diameter of $2r = 0.1\,\text{mm}$ are connected to the ground plane through lumped loads $Z = j\omega L$ with inductance L (actually, it is some effective inductance due to the presence of reactive parasitics considered in [18, 29]), and vertical PEC walls with a height of $v \le h$ and a thickness of 18 μm are placed between the adjacent pins. The two considered structures share the same periodicity and thickness, allowing a clear effect of the contribution of SD on the accelerated field decay, since the only difference between their macroscopic descriptions lies in the SD of the surface impedance.

Surface impedance as a function of γ is parametrically calculated in Computer Simulation Technology (CST) Studio Suite for both types of meta-atoms using periodic boundary conditions. The numerical results are shown in Fig. 3(b) with markers in good agreement with the analytical results obtained with (4). It validates the assumption that involving one pole and one zero (as supported by the approximation (4)) is sufficient to capture the main features of the surface impedance associated with both considered structures. At 10 GHz (above the quarter-wave resonance), the local MS (see the blue curve and markers) exhibits a high and γ-independent capacitive impedance $X/\eta \approx -3.5$ [30, Par. 11.4]. In contrast, for the nonlocal MS, the family of gray curves corresponding to $-3.5 \le A \le -0.5$ for fixed $B = 1$, $X/\eta = 3.5$ exhibits a common pole at $\gamma = 1$. This individual variation of A can be achieved in the proposed structure by adjusting v and L simultaneously. Details of the impedance extraction method and the correspondence obtained between v, L, and A are given in the SI Sec. 2. In particular, the case with $A \approx -3.5$ corresponds to $v = h = 6.2\,\text{mm}$ and $L = 0.63\,\text{nH}$ [see the red curve in Fig. 3(b)].

To further verify the analytically predicted field decay acceleration, we compared the numerically calculated electric-field profiles of the latter nonlocal MS (with $A = -3.5$) with the local one. With this aim, in CST Studio Suite (full-wave simulation with Frequency Domain Solver), we introduced a 2D HMD implemented as an internally fed open-ended parallel-plate waveguide with thickness $w = 0.18\,\text{mm}$ embedded in the center of the structure with finite size D (diameter along the x axis). This finite 1D row containing N meta-atoms is assumed

[4]The asymptotic expansion in (3) is formally derived under the assumption of large distances ($\Omega \gg 2\pi$); however, such asymptotic approximations often remain quantitatively accurate even at moderately large distances [10].

to be periodically repeated in the y direction. For both MSs, the open end is located in the top plane of the structure. To ensure the validity of the averaged boundary conditions, several closest meta-atoms at distances smaller than one period d from the source are removed, as schematically depicted in the inset of Fig. 3(d). The full-wave numerical results (markers) for $D = 12\lambda$ and $N = 118$ are compared with the analytical calculations (solid red and blue curves) in Fig. 2(a), showing good agreement. Note that at distances from the source $x/\lambda > 2$, the electric field decays by more than 70 dB, so that the expected decay profile $E_x \sim \Omega^{-5/2}$ cannot be confirmed for the practical structure due to the insufficient accuracy of numerical calculations (mainly caused by the effects of radiation boundaries). However, even at smaller distances, the advantage in field decay along the nonlocal MS of more than 25 dB is clearly reached compared to the local case.

One possible application of the observed effect is mitigating edge diffraction, which typically limits the shielding action of finite-sized antenna reflectors. To evaluate the role of SD, we compared the two structures described above with different diameters D. The shielding action can be quantified based on the far-field pattern using the so-called down-to-up ratio: $\mathrm{DU}(\phi) = H_y^{\mathrm{ff}}(-\phi)/H_y^{\mathrm{ff}}(\phi)$, where H_y^{ff} denotes the magnetic field in the far-field region and $\phi = \pi/2 - \theta$. As shown in the SI Sec. 3, $\mathrm{DU}(90^\circ)$ can be analytically estimated using the physical optics approach. While the magnetic field in the zenith ($\theta = 0^\circ$) is determined by $f_{H_y}(0^\circ)$, the field in the nadir ($\theta = 180^\circ$) can be approximated by the sum of two edge diffraction waves. The amplitude of both waves is proportional to the integral of the magnetic surface current density that would be induced by the HMD at an infinite MS (over the range of distances $D/2 \le |x| < \infty$, where the finite structure of diameter D is absent). For the nonlocal MS with $X/\eta \gg 1$ and $B = 1$ (the Norton wave suppressed), we can write:

$$\mathrm{DU}^{\mathrm{NL}}(90^\circ)\,[\mathrm{dB}] \approx 16.61 - 20\lg(1-A) - 50\lg kD. \quad (6)$$

A similar expression for the local HIS (with negative $\Im(Z_s)$ and $|X|/\eta \gg 1$), for which the Norton wave dominates at large distances, can be expressed as [10]:

$$\mathrm{DU}^{\mathrm{L}}(90^\circ)\,[\mathrm{dB}] \approx 1.05 - 30\lg kD. \quad (7)$$

The analytical estimates for the local and nonlocal MSs (for different negative A) are plotted in Fig. 3(c) versus D. As can be seen, the DU ratio in the nonlocal case with $A = -3.5$ can be reduced to -35 dB for a diameter of only one wavelength, which is by ≈ 14 dB better than that for the local HIS of the same size. Full-wave numerical simulations of local and nonlocal practical structures with $D = \lambda\,(N = 8)$ result in the $\mathrm{DU}(\phi)$ curves, shown in Fig. 3(d). An improvement of 10 dB can be observed at $\phi = 90^\circ$. A 4 dB deviation from the analytical estimation is due to the accuracy of the physical optics approximation and due to neglecting the contribution of the LW in the analytical estimation of the DU. Compared with a cardioid-shaped radiation pattern of a classical Huygens' source, both the local and nonlocal compact reflectors provide a steeper roll-off in the radiation pattern near the horizon ($\phi = 0^\circ$), which is beneficial in another important metric of shielding performance.

4. CONCLUSION

In this study, we investigate the tangential electric and magnetic field profiles excited on a nonlocal MS by a magnetic line current. At the macroscopic level, the MS is modeled using the second-order boundary conditions, whose coefficients fully characterize these field profiles. Among various coefficient combinations, a practically significant case arises when the surface impedance exhibits a second-order pole at grazing angles. The last property of the surface impedance demonstrates the possibility of accelerating field decay along nonlocal MSs with second-order SDs. Once the surface impedance has a pole at grazing angles, the contribution of the Norton wave in the asymptotic near-surface field expansion is suppressed. Although the contribution of the LW remains dominant near the HMD, the next nonzero higher-order term with profiles of $E_x \sim \Omega^{-5/2}$ and $H_y \sim \Omega^{-7/2}$ remains dominant at large distances from the source. The underlying physical intuition behind the accelerated field decay can be understood as follows. As demonstrated in [10], an effective way to mitigate edge effects is to minimize the equivalent currents flowing along the screen, thereby reducing the illumination of the edges by the MLC fields. Drawing from the concept of nonlocal radiation pattern engineering [18], one can observe that the introduction of a second-order pole in the SD of the surface impedance forces the radiation pattern to behave as $\cos^3\theta$ at $\theta \approx 90^\circ$. In contrast, a standard PMC boundary provides only a $\cos\theta$ dependence. Consequently, the nonlocal boundary can be expected to grant significantly lower edge illumination of a finite shield. In line with this concept, we have theoretically demonstrated that the condition $B = 1$ indeed yields the required enhanced field decay.

Found decay acceleration, in comparison to a local HIS (with the Norton wave prescribing the decay profile of $E_x \sim \Omega^{-3/2}$), can be achieved with the proposed practical periodic structure of inductively-loaded pins separated by metal walls, which is found to exhibit the required specific law of SD. The excitation of the proposed nonlocal MS as a wavelength-size reflector is associated with edge diffraction reduced by 10 dB compared to a state-of-the-art local MS reflector of the same size.

The proposed concept of Norton wave suppression via nonlocal MSs opens several promising research directions for future work. From a fundamental perspective, it enables further exploration of higher-order spatial dispersion and its impact on electromagnetic field behavior. Indeed, a pole of order N at the grazing angle would yield field decay scaling as $\Omega^{-(2N+1)/2}$ for the electric field and $\Omega^{-(2N+3)/2}$ for the magnetic field as follows from (3). However, the dispersion relation for surface impedance with such a pole order may contain up to $N+1$ solutions, making it challenging to address the contribution of all potentially excited guided waves without a dedicated study. Furthermore, the ability to shape tangential field distributions through the SD tailoring suggests potential applications in antenna decoupling. Indeed, the isolation of magnetic line currents placed above the suggested nonlocal MS at a distance of about two wavelengths can be improved in comparison to both PEC and PMC cases due to the rapid field [see Figs. 2(d), (e)]. To enhance the versatility of the proposed structure, the static

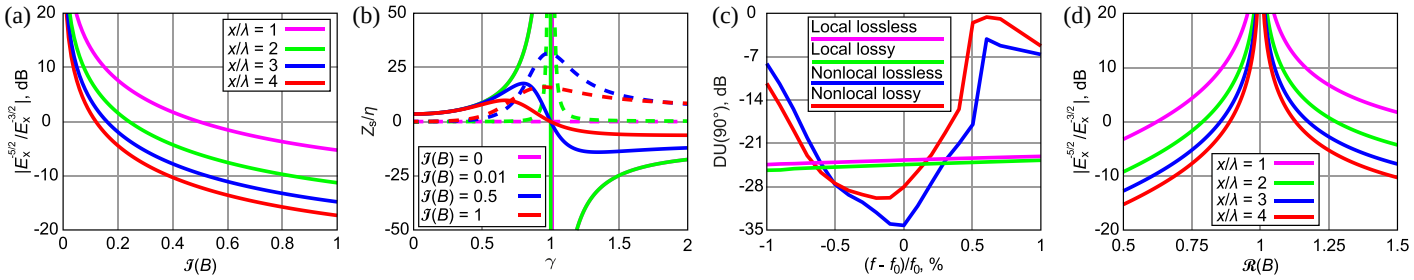

FIGURE A1. Practical issues of nonlocal MS implementation. (a) Ratio $|E_x^{-5/2}/E_x^{-3/2}|$ as a function of $\Im(B)$ at various points along the nonlocal MS. (b) Effect of $\Im(B)$ on the angular behavior of $Z_s(\gamma)$; solid lines denote the imaginary parts, and dashed lines denote the real parts. (c) Frequency dispersion of $\mathrm{DU}(90^\circ)$ for lossy and lossless structures under study. (d) Ratio $|E_x^{-5/2}/E_x^{-3/2}|$ as a function of B at various points along the nonlocal MS.

inductive elements can be replaced with parallel LC resonators. By employing voltage-tunable varactor diodes, the resonant frequency of the MS can be dynamically adjusted. This allows for real-time control over the wave-suppression characteristics, enabling the antenna to adapt to varying operational environments or frequency shifts.

From the application perspective, this approach can be extended to the design of compact antennas with enhanced shielding for Global Navigation Satellite Systems applications. However, three-dimensional antennas with circular polarization required in that application typically emit a superposition of transverse electric (TE) and transverse magnetic (TM) polarizations. For the TM component, enhanced field decay is anticipated. However, the algebraic asymptotic expressions of the fields should be derived in future work using 3D free-space Green's functions. Conversely, the TE component requires a separate, dedicated analysis to derive the SOBC coefficients necessary to ensure accelerated field decay for that polarization. Furthermore, it is important to address practically important issues, such as mitigating losses and improving bandwidth.

ACKNOWLEDGEMENT

The authors are thankful to Prof. Constantin Simovski for the useful discussions. This work was supported by the Russian Science Foundation (Project No. 25-19-00712, https://rscf.ru/en/project/25-19-00712/).

APPENDIX A. BANDWIDTH, LOSS EFFECTS, AND TOLERANCE ANALYSIS

In this Appendix, we present a study on bandwidth, loss effects, and fabrication tolerance analysis associated with the observed effect of the Norton wave suppression.

As follows from (5) and (4), losses in the structure can affect Norton wave suppression. For dissipative MSs, the approximation coefficients become complex-valued, and a nonzero $\Im(B)$ leads to the emergence of the Norton wave. To demonstrate the effect of nonzero $\Im(B)$, we gradually varied it while keeping $X/\eta = 3.5$, $A = -3.5$, and $\Re(B) = 1$, and examined the ratio $|E_x^{-5/2}|/|E_x^{-3/2}|$ (see Eq. (S.1) and Eq. (S.6) in the SI) as a function of $\Im(B)$ at various points along the nonlocal MS [see Fig. A1(a)]. It can be observed that for low losses (i.e., when the imaginary part of B is small), the Norton wave is suppressed. However, beyond a certain threshold of $\Im(B)$, it becomes significant and, with further increase in losses, eventually dominates along the surface. In addition, the Norton wave becomes more pronounced at larger distances, since the $x^{-5/2}$ component decays more rapidly. The plot (b) shows the angular dependence of the surface impedance for different values of $\Im(B)$. For very small losses, the surface impedance contains a clearly pronounced pole at grazing incidence. As losses increase, the pole near grazing incidence is smoothed out, leading to the emergence of the Norton wave.

To assess how losses affect the improved shielding performance, we simulated the same structures as in Section 3, replacing the PEC in the meta-atoms of the structures with copper. The down-to-up ratio at 90° increased from -34 dB to -30 dB at the target frequency f_0 [see Fig. A1(c)], which remains superior to that of the local structure (-24 dB). Remarkably, the losses do not significantly affect the local structure as it operates relatively far from the resonance. From the same plot, we can measure the fractional bandwidth of the nonlocal structure (defined as the frequency range where the nonlocal structure outperforms the local one) to be about 0.9%. In our recent paper [19], we found that nonlocal MSs tend to suffer from higher losses and narrower operating bandwidth than local ones. Therefore, it is an important topic to search for mechanisms to overcome these issues. Among different approaches, one may introduce additional degrees of freedom to the design [31] or implement MSs with simultaneously synthesized frequency and spatial dispersion [32].

Another important issue to address is sensitivity to fabrication tolerances. As follows from Table S.1 in the SI, the most critical parameters for tailoring spatial dispersion in the proposed nonlocal structure are the vias' inductance L and the wall height v. To study the sensitivity of the structure to these parameters, we varied their values within a range of $\pm 2.5\%$ around the nominal values. We found that this perturbation leads to a variation in the frequency at which $\Re(B) = 1$ of $\pm 0.5\%$. This means that the pole position slightly shifts, detuning the structure from the condition $B = 1$ at the operating frequency f_0. However, if the value of B lies in the acceptable range $[0.92, 1.08]$, the amplitude of the Norton wave is at least 3 dB smaller than that of the next algebraic term, as follows from Fig. A1(d).

REFERENCES

[1] Zenneck, J., "Über die Fortpflanzung ebener elektromagnetischer Wellen längs einer ebenen Leiterfläche und ihre Beziehung zur drahtlosen Telegraphie," *Annalen der Physik*, Vol. 328, No. 10, 846–866, 1907.

[2] Sommerfeld, A., "Über die Ausbreitung der Wellen in der drahtlosen Telegraphie," *Annalen der Physik*, Vol. 333, No. 4, 665–736, 1909.

[3] Norton, K. A., "The propagation of radio waves over the surface of the earth and in the upper atmosphere," *Proceedings of the Institute of Radio Engineers*, Vol. 24, No. 10, 1367–1387, 1936.

[4] Lalanne, P., J. P. Hugonin, and J. C. Rodier, "Theory of surface plasmon generation at nanoslit apertures," *Physical Review Letters*, Vol. 95, No. 26, 263902, 2005.

[5] Nikitin, A. Y., S. G. Rodrigo, F. J. García-Vidal, and L. Martín-Moreno, "In the diffraction shadow: Norton waves versus surface plasmon polaritons in the optical region," *New Journal of Physics*, Vol. 11, No. 12, 123020, Dec. 2009.

[6] Glybovski, S. B., S. A. Tretyakov, P. A. Belov, Y. S. Kivshar, and C. R. Simovski, "Metasurfaces: From microwaves to visible," *Physics Reports*, Vol. 634, 1–72, 2016.

[7] Kildal, P.-S., "Artificially soft and hard surfaces in electromagnetics," *IEEE Transactions on Antennas and Propagation*, Vol. 38, No. 10, 1537–1544, 1990.

[8] Sievenpiper, D., L. Zhang, R. F. J. Broas, N. G. Alexopolous, and E. Yablonovitch, "High-impedance electromagnetic surfaces with a forbidden frequency band," *IEEE Transactions on Microwave Theory and Techniques*, Vol. 47, No. 11, 2059–2074, 1999.

[9] Wait, J. R., "Excitation of surface waves on conducting, stratified, dielectric-clad, and corrugated surfaces," *Journal of Research of the National Bureau of Standards*, Vol. 59, No. 6, 365–377, 1957.

[10] Tatarnikov, D., V. Filippov, I. Soutiaguine, A. Astahov, A. Stepanenko, and P. Shamatulsky, "Multipath mitigation by conventional antennas with ground planes and passive vertical structures," *GPS Solutions*, Vol. 9, No. 3, 194–201, 2005.

[11] Baggen, R., M. Martinez-Vazquez, J. Leiss, S. Holzwarth, L. S. Drioli, and P. de Maagt, "Low profile GALILEO antenna using EBG technology," *IEEE Transactions on Antennas and Propagation*, Vol. 56, No. 3, 667–674, 2008.

[12] Scire-Scappuzzo, F. and S. N. Makarov, "A low-multipath wideband GPS antenna with cutoff or non-cutoff corrugated ground plane," *IEEE Transactions on Antennas and Propagation*, Vol. 57, No. 1, 33–46, 2009.

[13] Tatarnikov, D., A. Astakhov, and A. Stepanenko, "Broadband convex impedance ground planes for multi-system GNSS reference station antennas," *GPS Solutions*, Vol. 15, No. 2, 101–108, 2011.

[14] Yang, F. and Y. Rahmat-Samii, "Microstrip antennas integrated with electromagnetic band-gap (EBG) structures: A low mutual coupling design for array applications," *IEEE Transactions on Antennas and Propagation*, Vol. 51, No. 10, 2936–2946, 2003.

[15] Simovski, C., *Composite Media with Weak Spatial Dispersion*, Jenny Stanford Publishing, 2018.

[16] Luukkonen, O., C. Simovski, G. Granet, G. Goussetis, D. Lioubtchenko, A. V. Raisanen, and S. A. Tretyakov, "Simple and accurate analytical model of planar grids and high-impedance surfaces comprising metal strips or patches," *IEEE Transactions on Antennas and Propagation*, Vol. 56, No. 6, 1624–1632, 2008.

[17] Zhirihin, D., C. Simovski, P. Belov, and S. Glybovski, "Mushroom high-impedance metasurfaces for perfect absorption at two angles of incidence," *IEEE Antennas and Wireless Propagation Letters*, Vol. 16, 2626–2629, 2017.

[18] Zhuravlev, A., Y. Kurenkov, X. Wang, F. Dushko, V. Zalipaev, and S. Glybovski, "Radiation-pattern synthesis with uniform nonlocal metasurfaces," *Physical Review Applied*, Vol. 23, No. 4, 044052, Apr. 2025.

[19] Zhuravlev, A., S. Kuznetsov, D. Kiselkina, A. Shaham, A. Epstein, and S. Glybovski, "Wide-angle reflection suppression of dielectric slabs using nonlocal metasurface coatings," *IEEE Transactions on Antennas and Propagation*, 2026.

[20] Lindell, I. V., V. P. Akimov, and E. Alanen, "Image theory for dipole excitation of fields above and below a wire grid with square cells," *IEEE Transactions on Electromagnetic Compatibility*, Vol. 28, No. 2, 107–110, 1986.

[21] Felsen, L. B. and N. Marcuvitz, *Radiation and Scattering of Waves*, Wiley, Hoboken, NJ, USA, Jan. 1994.

[22] Maci, S. and A. Neto, "Green's function of an infinite slot printed between two homogeneous dielectrics — Part II: Uniform asymptotic solution," *IEEE Transactions on Antennas and Propagation*, Vol. 52, No. 3, 666–676, 2004.

[23] Maci, S., M. Caiazzo, A. Cucini, and M. Casaletti, "A pole-zero matching method for EBG surfaces composed of a dipole FSS printed on a grounded dielectric slab," *IEEE Transactions on Antennas and Propagation*, Vol. 53, No. 1, 70–81, 2005.

[24] Rahmeier, J. G. N., T. J. Smy, J. Dugan, and S. Gupta, "Zero thickness surface susceptibilities and extended GSTCs — Part I: Spatially dispersive metasurfaces," *IEEE Transactions on Antennas and Propagation*, Vol. 71, No. 7, 5909–5919, 2023.

[25] Dugan, J., T. J. Smy, F. Monticone, and S. Gupta, "Surface susceptibility synthesis of spatially dispersive metasurfaces for space compression and spatial signal processing," *IEEE Transactions on Antennas and Propagation*, Vol. 72, No. 8, 6572–6583, 2024.

[26] Tretyakov, S., *Analytical Modeling in Applied Electromagnetics*, Artech House, 2003.

[27] Silveirinha, M. G., C. A. Fernandes, and J. R. Costa, "Electromagnetic characterization of textured surfaces formed by metallic pins," *IEEE Transactions on Antennas and Propagation*, Vol. 56, No. 2, 405–415, 2008.

[28] Maslovski, S. I., T. A. Morgado, M. G. Silveirinha, C. S. R. Kaipa, and A. B. Yakovlev, "Generalized additional boundary conditions for wire media," *New Journal of Physics*, Vol. 12, No. 11, 113047, 2010.

[29] Kaipa, C. S. R., A. B. Yakovlev, S. I. Maslovski, and M. G. Silveirinha, "Mushroom-type high-impedance surface with loaded vias: Homogenization model and ultra-thin design," *IEEE Antennas and Wireless Propagation Letters*, Vol. 10, 1503–1506, 2011.

[30] Collin, R. E., *Field Theory of Guided Waves*, IEEE Press, 1990.

[31] Pfeiffer, C. and A. Grbic, "Bianisotropic metasurfaces for optimal polarization control: Analysis and synthesis," *Physical Review Applied*, Vol. 2, No. 4, 044011, Oct. 2014.

[32] Xu, G., S. V. Hum, and G. V. Eleftheriades, "Dual-band reflective metagratings with interleaved meta-wires," *IEEE Transactions on Antennas and Propagation*, Vol. 69, No. 4, 2181–2193, 2021.